Diagnosis of bubble evolution in laser-wakefield acceleration via angular distributions of betatron x-rays

Y. Ma,[1] L. M. Chen,[1,a)] N. A. M. Hafz,[2] D. Z. Li,[3] K. Huang,[1] W. C. Yan,[1] J. Dunn,[4] Z. M. Sheng,[2,5] and J. Zhang[2]
[1]*Beijing National Laboratory of Condensed Matter Physics, Institute of Physics, CAS, Beijing 100080, China*
[2]*Key Laboratory for Laser Plasmas and Department of Physics and Astronomy, Shanghai Jiao Tong University, Shanghai 200240, China*
[3]*Institute of High Energy Physics, CAS, Beijing 100049, China*
[4]*Lawrence Livermore National Laboratory, Livermore, California 94550, USA*
[5]*Department of Physics, Scottish Universities Physics Alliance, University of Strathclyde, Glasgow G4 0NG, United Kingdom*

(Received 7 September 2014; accepted 12 October 2014; published online 23 October 2014)

We present an indirect method to diagnose the electron beam behaviors and bubble dynamic evolution in a laser-wakefield accelerator. Four kinds of typical bubble dynamic evolution and, hence, electron beam behaviors observed in Particle-In-Cell simulations are identified correspondingly by simultaneous measurement of distinct angular distributions of the betatron radiation and electron beam energy spectra in experiment. The reconstruction of the bubble evolution may shed light on finding an effective way to better generate high-quality electron beams and enhanced betatron X-rays. © *2014 AIP Publishing LLC*. [http://dx.doi.org/10.1063/1.4900412]

In the laser-wakefield acceleration (LWFA),[1] the qualities of the accelerated electron beams are mainly determined by the dynamic evolution of the wakefield, especially in the bubble regime.[2,3] With a stable bubble structure formed under the matching condition $k_p w_0 = 2\sqrt{a_0}$,[4] where k_p is the plasma wave number, w_0 is the laser spot size and a_0 is the peak amplitude of the normalized vector potential of the laser field, high quality electron beams can be produced via self-injection. While, the departure from the matching condition usually causes instability of the bubble structure. The evolution of the bubble structure can induce multi-injection,[5–9] leading to large-energy spread beams. Meanwhile, the unstable evolution may cause transverse oscillations of the bubble structure, leading to collective transverse oscillations of the electron beam,[10,11] which will enlarge the divergence and the transverse emittance of the electron beam, and even shorten the dephasing length which eventually reduces the maximum energy gain of the beam. Therefore, it is necessary to study the dynamic evolution of the bubble to control the wakefield structure and hence the quality of the electron beam.

However, there is no direct method to diagnose the dynamic evolution of the bubble experimentally so far. Fortunately, we could still diagnose the bubble evolution and the behaviors of the electron beams indirectly with the aid of radiations emitted by the electron beams during the acceleration in the bubble. Betatron radiations are generated when the relativistic electrons perform transverse oscillations, referred to "betatron oscillations," due to the transverse focusing forces of the wakefiled,[12] resonant oscillations in the laser field,[13,14] and the unstable evolution of the bubble structure which is mentioned above.[6] The characteristics of the betatron radiation, such as photon flux, photon energy spectrum, angular distribution and the brilliance, are determined by the characteristics of the accelerated electron beam, such as beam charge, energy spectrum, amplitude of transverse oscillations, and beam duration,[15–17] and hence depend on the dynamic evolution of the wakefield. Therefore, by studying the characteristics of the betatron radiation, we can retrieve the behaviors of the electron beams, and, in principle, we can reconstruct the process of the bubble dynamic evolution.

In this letter, we found through 2D-Particle-In-Cell (PIC) simulations that for different laser-plasma parameters and at different stages of the bubble evolution, there are four different distinct bubble structures. These four kinds of bubble structures result in four kinds of different electron beam energy spectra and transverse oscillations, respectively, and hence different angular distributions of the betatron radiation. These simulations are confirmed experimentally from the betatron radiation of multi-hundred MeV wakefield-accelerated electron beams. By analyzing the angular distributions of the betatron radiation and the electron beam energy spectra, the injection regime of the electron beams and their transverse oscillations behaviors were identified and the dynamic evolution of the bubble structure were reconstructed.

PIC simulations were carried out with the 2D PIC code OOPIC.[18] The simulation box with a moving window is $100\,\mu\text{m} \times 160\,\mu\text{m}$ corresponding to 500×4000 cells in y and x directions, and each cell contains 9 macro particles. The spatial and temporal distribution of the laser pulse can be expressed as $a(\tau, y) = a_0 \sin(2\pi\tau/3\tau_L)\exp(-y^2/w_0^2)\cos(2\pi\tau/T)$ for $0 < \tau < 3/2\tau_L$, where $\tau = t - x/c$ with c the speed of light, $a_0 = 3.64$, $\tau_L = 60$ fs is the full width at half maximum (FWHM) pulse duration, $w_0 = 18\,\mu\text{m}$ is the $1/e^2$ spot radius and $T = \lambda_L/c$ with $\lambda_L = 800\,\text{nm}$. The intensity of the laser pulse is $I = 2.83 \times 10^{19}\,\text{W/cm}^2$, and the power of the laser pulse is 144 TW. The drive laser pulse is launched into homogeneous plasma in x direction and linearly polarized in y direction.

a)Author to whom correspondence should be addressed. Electronic mail: lmchen@iphy.ac.cn

Four kinds of bubble structures are shown in Figs. 1(a)–1(d). First, in the bubble regime, the pondermotive force of a strong laser pulse ($a_0 \gg 1$) is responsible for the formation of the bubble. As shown in Fig. 1(a), electrons which are expelled by the laser pondermotive force flow backwards to the rear of the bubble and then are self-injected. During the acceleration, electrons perform transverse oscillations due to the transverse focusing force. The pondermotive force is isotropic in the transverse direction, so do the transverse oscillations of the self-injected electron beam. The divergence angles of the betatron radiation in the oscillation plane and the plane perpendicular to the oscillation are $\theta_y = K/\gamma$ and $\theta_z = 1/\gamma$, respectively,[16] where $K = \gamma\omega_\beta r_\beta/c$ is a parameter describing the strength of betatron oscillations, γ is the Lorenz factor, $\omega_\beta = \omega_p/\sqrt{2\gamma}$ is the betatron oscillations frequency, ω_p is the plasma frequency, and r_β is the amplitude of the betatron oscillations. Generally speaking, $K \gg 1$ is satisfied with $\gamma > 100$ and $r_\beta > 1\,\mu$m. Therefore, $\theta_y > \theta_z$ is usually satisfied. Since the transverse oscillation of the self-injected electron beam is isotropic, the angular distribution of the betatron radiation is also isotropic.

Second, when the plasma density is slightly higher than that of the matching condition, an unstable state of the bubble structure emerges, as shown in Fig. 1(b). During the interaction, the laser pulse front is eroded gradually, leading to the shortening of the pulse duration and the increase in the laser intensity which eventually causes a longitudinal stretch of the bubble and a continuous injection of the second bunch.[19] Moreover, when the laser pulse duration is short enough, the carrier envelope phase effects dominate and the pondermotive approximation breaks down. As a result, the plasma response to the laser field becomes asymmetrical because of the variation of the carrier envelope phase and causes the transverse oscillations of the bubble[10] in the plane of the laser polarization, i.e., x-y plane in Fig. 1. The oscillations of the second electron bunch induced by the bubble oscillations are also along the y direction, and hence, the angular distribution of the betatron radiation emitted by this electron bunch should be anisotropic. When the oscillations of the bubble occur, the acceleration of the first electron bunch has already stopped and electrons start to dephase. The bubble oscillations have little influence on the motion of the first bunch as well as the betatron radiation emitted by it, leading to an isotropic angular distribution of the betatron radiation emitted by this electron bunch. Therefore, the spatial distribution of the betatron radiation is composed of two different parts. The transverse profiles of the radiation at far field should be a circle rounded by an ellipse or otherwise, depend on the difference of the energies and oscillation amplitudes between these two electron bunches, according to the formula $\theta = K/\gamma = \omega_p r_\beta/c\sqrt{2\gamma}$.

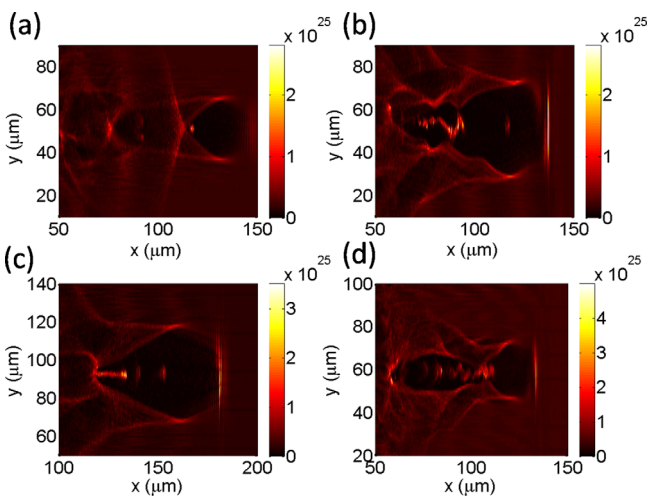

FIG. 1. Plasma density distributions in PIC simulations. (a) Generation of a stable bubble and mono-energetic electron beam under the matching condition with $a_0 = 3.64$, $\tau = 60$ fs, $w_0 = 18\,\mu$m, and plasma density $n_p = 1.5 \times 10^{18}\,\text{cm}^{-3}$. (b) Oscillations of the bubble structure and the second electron bunch when only changes the plasma density to $n_p = 2.0 \times 10^{18}\,\text{cm}^{-3}$ after laser pulse propagates 8.7 mm while the dephasing length of the first electron beam is $L_d = 6.3$ mm. (c) Generation of an elongated bubble but without the oscillations of the bubble structure and the continuously injected electron bunch when $n_p = 2.0 \times 10^{18}\,\text{cm}^{-3}$ and $w_0 = 36\,\mu$m, while maintains other parameters unchanged in (a). (d) An oscillating bubble causes the oscillation of the continuously injected electron bunch after the laser propagates 5 mm when $n_p = 5.0 \times 10^{18}\,\text{cm}^{-3}$, while the other parameters in (a) remain the same.

When the laser spot radius is enlarged to twice that of in Fig. 1(b) (in this case, the simulation box is enlarged to $180\,\mu\text{m} \times 200\,\mu\text{m}$ with 900×5000 cells in y and x directions), the oscillations of the continuously injected electron bunch in the y direction are suppressed, as shown in Fig. 1(c). This is because of the fact that, during such a continuous injection, the carrier envelope phase effects on the interaction are not significant and the shortening of the laser pulse has already caused a stretching of the bubble longitudinally. Therefore, we expect that the angular distribution of the betatron radiation generated in this case should be isotropic.

Finally, by choosing a much higher plasma density than that of the matching condition, the pump depletion happens faster because the pump depletion length L_{etch} is inversely proportional to the plasma density n_p according to the formula $L_{etch} \approx c\tau_L\omega_0^2/\omega_p^2 \propto 1/n_p$,[4] where ω_0 is the laser frequency in vacuum. In this situation, the laser pulse shortening starts very early, and a large number of electrons are injected into the oscillating bubble continuously and perform collective oscillations in the polarization plane, as shown in Fig. 1(d), producing an anisotropic distributed betatron radiation.

Thus, these four kinds of beam behaviors and bubble structure evolution can be diagnosed experimentally by analyzing the betatron beam profiles combined with the electron beam energy spectra in principal. In fact, the assumption has been confirmed by a well designed experiment which is discussed in detail in the following part.

The experiment was performed at the Jupiter Laser Facility, Lawrence Livermore National Laboratory, using Callisto laser system.[6] This laser system delivers up to 200 TW in power with a FWHM pulse duration of 60 fs at the central wavelength of 806 nm. The laser pulse was focused by an $f/12$ off-axis parabola to a focal spot of 18 μm with 35% energy concentration. The peak power ranged from 60 TW to 155 TW on target. The laser intensity ranged from $1.1 \times 10^{19}\,\text{W/cm}^2$–$3.0 \times 10^{19}\,\text{W/cm}^2$, corresponding to a_0 of 2.3–3.8. A supersonic helium gas jet with a rectangular nozzle of size $10\,\text{mm} \times 1.2\,\text{mm}$ was used, which could

produce well defined uniform gas density profiles from $1.0 \times 10^{18}\,\mathrm{cm}^{-3}$ to $3.0 \times 10^{19}\,\mathrm{cm}^{-3}$.[20]

The experimental results are shown in Figs. 2 and 3. Figs. 2(a)–2(d) show the electron beam energy spectra and the corresponding spatial profiles of the betatron X-rays in same shots in different color scales, while Figs. 3(a)–3(d) show the detailed angular distributions in the y and z directions using Gaussian fitting.

In the first case, as shown in Fig. 2(a), a quasi-monoenergetic electron beam together with a circular betatron X-ray profile are generated. Gaussian fitting show that the betatron X-ray is confined in a cone of $\theta_y \times \theta_z = 10$ mrad $\times$ 10 mrad, as shown in Fig. 3(a), where θ_y and θ_z are the FWHM divergence angles in the y and z directions, respectively. From the isotropic betatron X-ray profile, we can infer that the transverse oscillations of the electron beam are also isotropic. Taking into account the quasi-monoenergetic electron beam energy spectrum, which is shown in Fig. 2(e), we can come to the conclusion that, in this situation, the bubble structure is very stable and self-injected electrons perform isotropic transverse oscillations during the acceleration, as illustrated in Fig. 1(a).

The profile of the betatron X-ray in Fig. 2(b) is more complicated, i.e., a brighter circular core surrounded by a dimmer ellipse. We believe that the radiation with such kind of profile is composed of two different parts. The superposition of the Gaussian fitting of each part in the y direction is well consistent with experimental results, as shown in Fig. 3(b). The FWHM divergence angles of the elliptical surroundings and the circular core in the y direction are $\theta_{y1} = 30$ mrad and $\theta_{y2} = 10$ mrad, respectively, while nearly the same

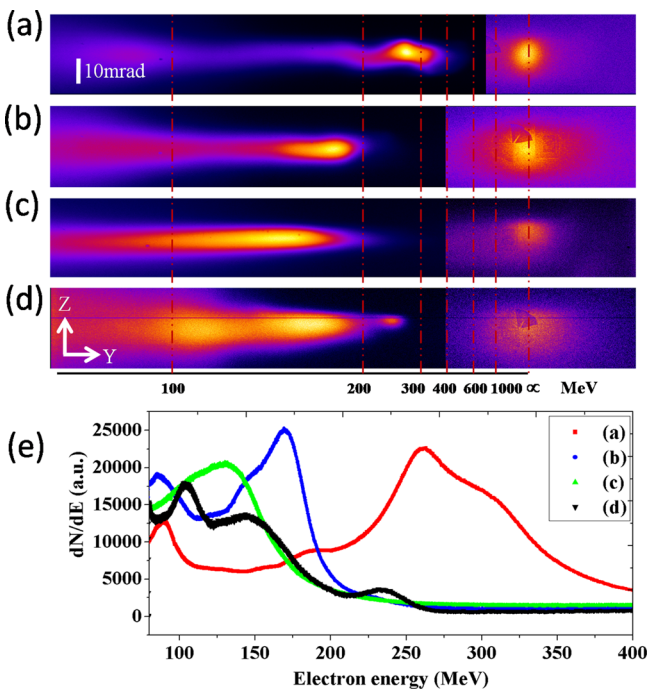

FIG. 2. (a)–(d) show the energy distributions of the electron beams and the profiles of the betatron X-rays in image plates with different color scale, and (e) gives the corresponding electron beam energy spectra of (a)–(d). The laser energy and plasma density in each shot are (a) $E_L = 6.5$ J, $n_p = 4.0 \times 10^{18}\,\mathrm{cm}^{-3}$, (b) $E_L = 4.9$ J, $n_p = 3.8 \times 10^{18}\,\mathrm{cm}^{-3}$, (c) $E_L = 6.8$ J, $n_p = 4.6 \times 10^{18}\,\mathrm{cm}^{-3}$, and (d) $E_L = 4.8$ J, $n_p = 4.2 \times 10^{18}\,\mathrm{cm}^{-3}$, respectively.

in the z direction which are $\theta_{z1} \approx \theta_{z2} = 10$ mrad, as shown in the inset of Fig. 3(b), where the subscripts 1, 2 denote the outer part and the inner part of the radiation, respectively. Such kind of profile can only be explained by the assumption that different parts in the radiation come from different electron beams, i.e., the inner circle comes from an isotropic transversally oscillated beam, and the outer ellipse comes from an electron beam which performs dominating oscillations in the y direction. This assumption is supported by the electron beam energy spectrum shown in Figs. 2(b) and 2(e), which is composed of a mono-energetic part peaked at 175 MeV and a continuous part below 150 MeV if it is true that the monoenergetic bunch oscillates isotropically while the continuous bunch oscillates anisotropically, as the situation of Fig. 1(b), although the oscillating behaviors of the beam cannot be retrieved from the electron beam energy spectrum alone. In other words, the oscillations, no matter isotropic or anisotropic, could be diagnosed indirectly by analyzing the spatial profiles of the betatron radiation. In addition, the amplitude of the transverse oscillations can be obtained according to the formula $\theta = K/\gamma = \omega_p r_\beta / c\sqrt{2\gamma}$ as follows:

$$\frac{\theta_{y1}}{\theta_{y2}} = \frac{r_{\beta y1}}{r_{\beta y2}} \sqrt{\frac{\gamma_2}{\gamma_1}} = 3, \tag{1}$$

$$\frac{\theta_{z1}}{\theta_{z2}} = \frac{r_{\beta z1}}{r_{\beta z2}} \sqrt{\frac{\gamma_2}{\gamma_1}} = 1. \tag{2}$$

The isotropy of the inner part of the radiation gives

$$r_{\beta y2} = r_{\beta z2}. \tag{3}$$

Thus,

$$\frac{r_{\beta y1}}{r_{\beta z1}} = 3, \tag{4}$$

which illustrates the anisotropy of the transverse oscillations of the continuously injected electron bunch.

In the third case, similar to that in Fig. 2(a), the profile of the betatron radiation in Fig. 2(c) is nearly a circle with $\theta_y = 14$ mrad and $\theta_z = 12$ mrad, as shown in Fig. 3(c), which illustrates a nearly isotropic oscillation of the electron beam. However, the continuous electron beam energy spectrum in this case, as shown in Fig. 2(c), is quite different with that of the first case in Fig. 2(a). These two characteristics, i.e., the isotropy of the electron beam oscillations and the continuity of the electron beam energy spectrum, are exactly what are depicted in the simulations results in Fig. 1(c).

Compared with Fig. 2(c), the electron beam energy spectrum in Fig. 2(d) is also continuous, but the profile of the betatron radiation is elliptical, with $\theta_y = 30$ mrad and $\theta_z = 20$ mrad, as shown in Fig. 3(d). The underlying physics in this situation is that, during the continuous injection and the acceleration process, electron beam performs anisotropic oscillations which dominate in the laser polarization plane, just as illustrated in Fig. 1(d) in simulations.

The significant differences between these four situations are due to slight changes in laser and plasma parameters, as described in the caption of Fig. 2, which means that the bubble evolution and the behaviors of the electron beams are

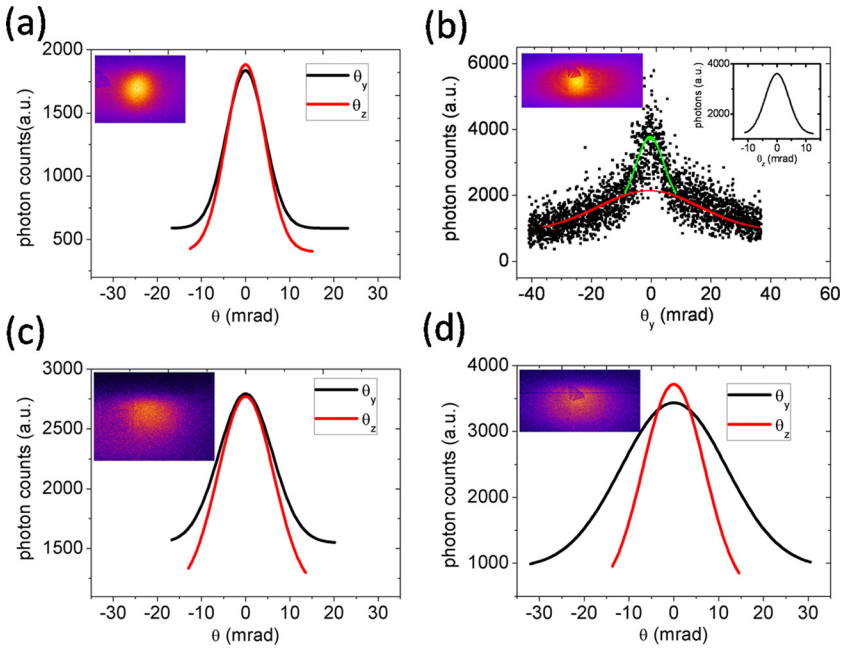

FIG. 3. Gaussian fitting of the profile of the betatron radiation. In (a), (c), and (d), the black solid line represents the direction of laser polarization and the red solid line represents the directions perpendicular to laser polarization. In (b), black dots show the raw data of the betatron photons in the *y* direction which is fitting by two independent Gaussian curves. The green solid line fits the brighter inner part and the red solid line fits the dimmer outer part, respectively. The inset of (b) represents the fitting in the *z* direction. Since the divergence angles in the *z* direction of these two parts are nearly the same, so we use a single curve here to give the divergence angles.

very sensitive to the changes of the experimental parameters. Therefore, in order to better control the quality of the electron beams and to enhance the betatron radiation, it is necessary to diagnose the bubble evolution precisely.

We thank R. Cauble, S. Maricle, J. Bonlie, and other Jupiter Laser Facility staffs at Lawrence Livermore National Laboratory (LLNL) for laser and technical support and Joseph Nilsen for facilitating the experiment. This work was supported by the National Basic Research Program of China (Nos. 2013CBA01501 and 2013CBA01504), National key Scientific Instrument and Equipment Development Project (No. 2012YQ120047), and the National Natural Science Foundation of China (Nos. 60878014, 10974249, 10925421, 11105217, 11121504, 11175119, and 11175192).

[1]T. Tajima and J. M. Dawson, Phys. Rev. Lett. **43**, 267 (1979).
[2]A. Pukhov and J. Meyer-ter Vehn, Appl. Phys. B **74**, 355 (2002).
[3]I. Kostyukov, A. Pukhov, and S. Kiselev, Phys. Plasmas **11**, 5256 (2004).
[4]W. Lu, M. Tzoufras, C. Joshi, F. S. Tsung, W. B. Mori, J. Vieira, R. A. Fonseca, and L. O. Silva, Phys. Rev. Spec. Top. Accel. Beams **10**, 061301 (2007).
[5]A. Oguchi, A. Zhidkov, K. Takano, E. Hotta, K. Nemoto, and K. Nakajima, Phys. Plasmas **15**, 043102 (2008).
[6]W. C. Yan, L. M. Chen, D. Z. Li, L. Zhang, N. A. M. Hafz, J. Dunn, Y. Ma, K. Huang, L. Su, M. Chen, Z. M. Sheng, and J. Zhang, Proc. Natl. Acad. Sci. **111**,5825 (2014).
[7]H. Yoshitama, T. Kameshima, Y. Q. Gu, Y. Guo, C. Y. Jiao, H. J. Liu, H. S. Peng, C. M. Tang, X. D. Wang, X. L. Wen *et al.*, Chin. Phys. Lett. **25**, 2938 (2008).
[8]S. Y. Kalmykov, A. Beck, S. A. Yi, V. N. Khudik, M. C. Downer, E. Lefebvre, B. A. Shadwick, and D. P. Umstadter, Phys. Plasmas **18**, 056704 (2011).
[9]N. A. M. Hafz, S. K. Lee, T. M. Jeong, and J. M. Lee, Nucl. Instrum. Methods Phys. Res., Sect. A **637**, S51 (2011).
[10]E. N. Nerush and I. Yu. Kostyukov, Phys. Rev. Lett. **103**, 035001 (2009).
[11]A. Popp, J. Vieira, J. Osterhoff, Zs. Major, R. Horlein, M. Fuchs, R. Weingartner, T. P. Rowlands-Rees, M. Marti, R. A. Fonseca *et al.*, Phys. Rev. Lett. **105**, 215001 (2010).
[12]A. Rousse, K. Ta Phuoc, R. Shah, A. Pukhov, E. Lefebvre, V. Malka, S. Kiselev, F. Burgy, J. P. Rousseau, D. Umstadter, and D. Hulin, Phys. Rev. Lett. **93**, 135005 (2004).
[13]S. Cipiccia, M. R. Islam, B. Ersfeld, R. P. Shanks, E. Brunetti, G. Vieux, X. Yang, R. C. Issac, S. M. Wiggins, G. H. Welsh *et al.*, Nat. Phys. **7**, 867 (2011).
[14]F. Albert, B. B. Pollock, J. L. Shaw, K. A. Marsh, J. E. Ralph, Y.-H. Chen, D. Alessi, A. Pak, C. E. Clayton, S. H. Glenzer, and C. Joshi, Phys. Rev. Lett. **111**, 235004 (2013).
[15]E. Esarey, B. A. Shadwick, P. Catravas, and W. P. Leemans, Phys. Rev. E **65**, 056505 (2002).
[16]S. Corde, K. Ta Phuoc, G. Lambert, R. Fitour, V. Malka, and A. Rousse, Rev. Mod. Phys. **85**, 1 (2013).
[17]K. Nakajima, A. H. Deng, X. M. Zhang, B. F. Shen, J. S. Liu, R. X. Li, Z. Z. Xu, T. Ostermayr, S. Petrovics, C. Klier *et al.*, Phys. Rev. Spec. Top. Accel. Beams **14**, 091301 (2011).
[18]J. P. Verboncoeur, A. B. Langdon, and N. T. Gladd, Comput. Phys. Commun. **87**, 199 (1995).
[19]Y. Ma, L. M. Chen, and M. Chen, "Generation of brilliant femtosecond Gamma-ray burst stimulated by laser-driven hosing instabilities" (unpublished).
[20]T. Hosokai, K. Kinoshita, T. Watanabe, K. Yoshii, T. Ueda, A. Zhidokov, M. Uesaka, K. Nakajima, M. Kando, and H. Kotaki, in *Proceedings of the European Particle Accelerator Conference* (2002), pp. 981–983.